FULL PAPER

PPS www.rsc.org/pps

Laser-assisted fluorescence microscopy for measuring cell membrane dynamics

Herbert Schneckenburger,[a,b] Michael Wagner,[a] Martina Kretzschmar,[a] Wolfgang S. L. Strauss[b] and Reinhard Sailer[b]

[a] *Fachhochschule Aalen, Institut für Angewandte Forschung, Beethovenstr. 1, 73430 Aalen, Germany*

[b] *Institut für Lasertechnologien in der Medizin und Messtechnik an der Universität Ulm, Helmholtzstr. 12, 89081 Ulm, Germany*

Received 5th January 2004, Accepted 17th May 2004
First published as an Advance Article on the web 28th May 2004

Membranes of living cells are characterized by laser-assisted fluorescence microscopy, in particular a combination of microspectrofluorometry, total internal reflection fluorescence microscopy (TIRFM), fluorescence lifetime imaging (FLIM) and Förster resonance energy transfer (FRET) spectroscopy. The generalized polarization (GP, characterizing a spectral shift which depends on the phase of membrane lipids) as well as the effective fluorescence lifetime (τ_{eff}) of the membrane marker laurdan were revealed to be appropriate parameters for membrane stiffness and fluidity. GP decreased with temperature, but increased during cell growth and was always higher for the plasma membrane than for intracellular membranes. Microdomains of different fluorescence lifetimes τ_{eff} were observed at temperatures above 30 °C and disappeared during cell aging. Non-radiative energy transfer was used to detect laurdan selectively in close proximity to a molecular acceptor (DiI) and may present a possibility for measuring membrane dynamics in specific microenvironments.

Introduction

Fluorescence techniques are widespread in the field of biomedical diagnostics,[1,2] since in addition to some intrinsic fluorophores[3–5] numerous dyes for staining cell nuclei, membranes or subcellular organelles as well as for probing ion concentrations, pH values or membrane potentials have become available.[6,7] In addition, green fluorescent proteins (GFPs) and their mutants are used for site-specific tracking of living cells or organisms.[8,9] Fluorescence microscopy is probably the most commonly used method, which is increasingly combined with laser excitation.

In comparison with conventional light sources, lasers offer several advantages: (1) coherence, which is used for interferometry or holography; (2) focusing abilities to a diffraction limited spot with a radius $r = 0.61\ \lambda/A$ with λ corresponding to the wavelength of radiation and A to the numerical aperture of the focusing lens, *e.g.* microscope objective lens; (3) high spectral resolution of 10^{-5} nm $\leq \Delta\lambda \leq$ 1 nm; (4) high temporal resolution with pulse widths of 4 fs $\leq \Delta t \leq$ 20 ns.

Generally, wide field fluorescence microscopy and (confocal[10] or multiphoton[11,12]) laser scanning microscopy are important, both permitting high spatial, spectral and temporal resolution, when monochromatic laser light is focused to the micrometer or sub-micrometer range. The present article is focused on applications of wide-field microscopy to the fluorescent membrane marker laurdan including microspectrofluorometry, total internal reflection fluorescence microscopy (TIRFM), fluorescence lifetime imaging (FLIM) and Förster resonance energy transfer spectroscopy (FRET). Time-resolving (nanosecond and subnanosecond) techniques are emphasized, since the fluorescence lifetime of a molecule may be sensitive to its microenvironment and gives therefore valuable information on its molecular or cellular interactions. The fluorescence lifetime τ can be described as the reciprocal of the sum of all rates k_i deactivating an excited molecular state, in particular the rate of fluorescence (k_F) and the rates of non-radiative transitions, *e.g.* internal conversion (k_{IC}), singlet–triplet intersystem crossing (k_{ISC}) and energy transfer to adjacent molecules (k_{ET}) according to[2]

$$k = k_F + k_{IC} + k_{ISC} + k_{ET} = 1/\tau \qquad (1)$$

Therefore, τ is sensitive to changes of internal conversion due to specific molecular interactions or to intermolecular energy transfer.

All experimental methods were used for studies of membrane dynamics of Chinese hamster ovary (CHO) cells incubated with the fluorescent membrane marker laurdan (6-dodecanoyl-2-dimethylamino-naphthalene, Fig. 1). This dye is a polarity-sensitive probe, whose electronic excitation energy is different in polar and non-polar environments.[13,14] Once incorporated into cell membranes, the fluorescence of this probe shows a spectral shift to longer wavelengths when its molecules are in contact with adjacent water molecules, *e.g.* when a phase transition from the tightly packed gel phase to the liquid crystalline phase of membrane lipids occurs. In addition, the fluorescence lifetime of laurdan has been reported to depend on membrane dynamics.[15] Therefore, fluorescence spectra and lifetime images of cultivated CHO cells incubated with laurdan are examined as a function of temperature, age and growth phase of the cells. Differences between the plasma membrane (assessed by TIRFM) and intracellular membranes (assessed by illumination of whole cells) are emphasized.

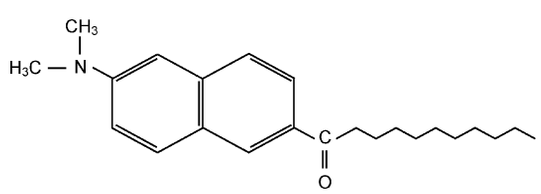

Fig. 1 Chemical structure of the 6-dodecanoyl-2-dimethylamino-naphthalene (laurdan) molecule.

Materials and methods

Cells

CHO-K1 hamster ovary cells were routinely cultured in F-10 HAM nutrient mixture supplemented with 10% fetal calf serum (FCS), 7.5% sodium bicarbonate and antibiotics at 37 °C and

DOI: 10.1039/b317047k

5% CO_2. After seeding of 150 cells mm^{-2}, cells were grown on microscope object slides for either 24 or 48 h prior to incubation for 60 min with 8 μM laurdan diluted in culture medium. After a growth period of 48 h a sub-confluent cell monolayer was obtained, whereas individual cells and small cell clusters were predominant after 24 h. After incubation cells were rinsed with PBS and measured in an open aluminium chamber at variable temperatures ranging from 24 to 41 °C using a 63×/0.90 water immersion objective lens. The chamber (filled with a layer of 2–3 mm PBS) contained a pair of high-power resistors for heating as well as a calibrated thermocouple which was controlled by a microprocessor and placed in close vicinity to the measured part of the sample. Measurements were performed with two groups of subcultures (SC): SC 12–23 ('young cells') and SC 35–38 ('aged cells'). Measurements which are not further specified, were carried out with SC 12–23.

For energy transfer (FRET) measurements in the plasma membrane, cells were coincubated for 10 min with laurdan (8 μM) and DiI (1,1′-dioctadecyl-3,3,3′,3′-tetramethyl-indocarbocyanine perchlorate; 2, 4 or 8 μM), which has also been described as a membrane marker.[16] The short incubation time in this case was optimized for the detection of DiI fluorescence in the plasma membrane. Cells incubated solely with laurdan were used as a reference.

Microspectrofluorometry

Fluorescence of laurdan was excited at 391 nm, which corresponds to its absorption maximum when incorporated into cell membranes in their gel phase. However, efficient excitation of laurdan is also achieved in the liquid crystalline phase of membrane lipids at the same wavelength.[15] A picosecond laser diode (LDH 400 with driver PDL 800-B, Picoquant, Berlin, Germany; pulse energy: 12 pJ, pulse duration: 55 ps, repetition rate: 40 MHz; average power: 0.5 mW) was used in combination with a single mode fiber system (Point Source, kineFlex-p-3-S-395, Southampton, UK) and a custom-made dark field condensor adapted to the fluorescence microscope (Axioplan 1, Carl Zeiss Jena, Germany), as depicted in Fig. 2. This condensor permitted a variation of the angle of incidence of the excitation light above and below the critical angle (Θ_C = 64.9°) for total internal reflection.[17] Therefore, Θ = 62° was used for illumination of whole cells, whereas Θ = 66° was used for selective illumination of the plasma membrane (by an evanescent electromagnetic field, see below). Due to attenuation by the fiber and its collimating optics the average light power in the plane of the sample was limited to about 35 μW. Fluorescence spectra were detected using a polychromator and an image intensifying system (IMD D4562, Hamamatsu Photonics, Ichino-Cho, Japan)[18] fixed on top of the microscope (not shown in Fig. 2).

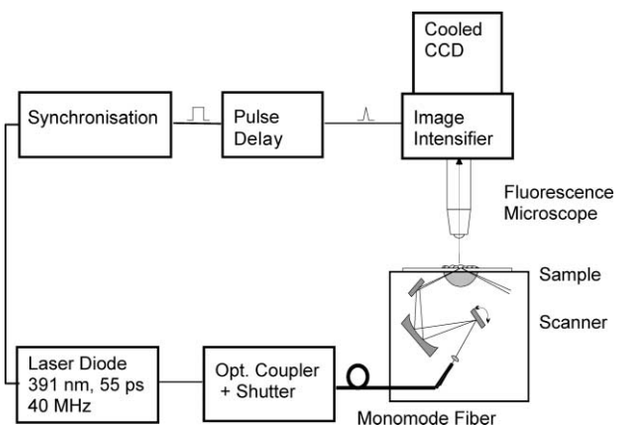

Fig. 2 Experimental setup for fluorescence lifetime imaging (FLIM) with variable-angle excitation.

Total internal reflection fluorescence microscopy (TIRFM)

TIRFM is based on total internal reflection of a light beam propagating through a medium of refractive index n_1 and meeting an interface to a second medium of refractive index $n_2 < n_1$. Total internal reflection occurs at all angles of incidence Θ, which are greater than the critical angle $\Theta_C = \arcsin(n_2/n_1)$. Despite being totally reflected the incident light beam evokes an evanescent electromagnetic field that penetrates into the second medium and decays exponentially with perpendicular distance z from the interface according to $I(z) = I_0\, e^{-z/d(\Theta)}$. $I(z)$ corresponds to the intensity of the electromagnetic field and $d(\Theta)$ to the penetration depth at wavelength λ, as given by[19]

$$d(\Theta) = (\lambda/4\pi)\,(n_1^2 \sin^2\Theta - n_2^2)^{-1/2} \qquad (2)$$

When using an excitation wavelength of 391 nm, n_1 = 1.535 corresponds to the glass substrate (hemicylindrical prism) and n_2 = 1.39 to the cytoplasm, resulting in Θ_C = 64.9°. The illumination device depicted in Fig. 2 permits continuous variation of the angle of incidence Θ and therefore of the penetration depth d, such that *e.g.* cell-substrate topologies can be examined.[17] For the present application only fixed values (see above) were used for excitation of either whole cells or plasma membranes (and its adjacent cellular sites with a penetration depth of about 160 nm).

Fluorescence lifetime imaging (FLIM)

In general, fluorescence profiles are recorded using picosecond lasers and ultrafast detection devices. Kinetics of fluorescence increase and decay are fitted by single or multiple exponential functions with well defined time constants corresponding to the fluorescence rise times and lifetimes, respectively. Alternatively, *effective* fluorescence lifetimes τ_{eff} can be calculated from the intensities I_1 and I_2 measured in two time gates of identical width and a time shift Δt between each other according to the formula[20]

$$\tau_{eff} = \Delta t/\ln(I_1/I_2) \qquad (3)$$

Only when fluorescence decay kinetics are monoexponential, τ_{eff} corresponds to the real fluorescence lifetime; if kinetics are multiexponential, τ_{eff} depends on all time constants of fluorescence increase and decay.

In the present experiments fluorescence images were recorded using an image intensifying camera system (Picostar HR 12 image intensifier coupled to a cooled ICCD camera; LaVision, Göttingen, Germany) with a time gate of 200–1000 ps width and adjustable delay times. As depicted in Fig. 2, the electrical output signal of the laser diode was used for synchronization. Images were recorded either in a continuous wave (cw) mode or within the time intervals of 1–2 ns (I_1) as well as 4–5 ns (I_2) after each laser pulse. Acquisition times of 1 s were used for illumination of whole cells (Θ = 62°), whereas acquisition times of 10 s were used for selective illumination of plasma membranes (Θ = 66°). Fluorescence lifetime images were calculated according to eqn. (3) and are depicted for whole cell illumination.

Förster resonance energy transfer (FRET)

Energy transfer by direct interaction of optical transition dipoles of a donor and an acceptor molecule is a mechanism of significant analytical importance. The dipole–dipole interaction is proportional to r^{-6} with r being the intermolecular distance and requires an overlap of the emission spectrum of the donor and the absorption spectrum of the acceptor according to

$$k_{ET} \approx r^{-6} \int \varepsilon_A(\nu)\, I_D(\nu)\, \nu^{-4}\, d\nu \qquad (4)$$

with k_{ET} being the rate of energy transfer, $\varepsilon_A(\nu)$ the molar extinction coefficient of the acceptor, $I_D(\nu)$ the flux of emitted photons of the donor and ν the frequency of radiation. Light is absorbed by the donor and emitted by the acceptor, whereas the intermolecular energy transfer is non-radiative.

The principle of this so-called Förster mechanism[21] is exemplified in Fig. 3 (upper part) for the donor–acceptor pair laurdan ⟶ DiI. The emission spectrum of laurdan and the absorption spectrum of DiI are depicted in the lower part of this figure. The spectral overlap indicates that the condition of resonance is fairly fulfilled. Since FRET is limited to intermolecular distances of a few nanometers, the method may be used to probe a donor species in close vicinity of an acceptor molecule or to quantify donor–acceptor interactions.

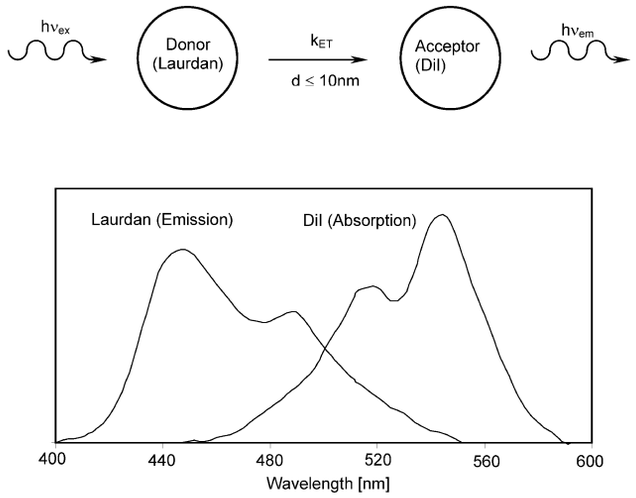

Fig. 3 Principle of non-radiative energy transfer in cell membranes from laurdan to DiI (top); emission spectrum of laurdan and absorption spectrum of DiI (bottom).

Energy transfer rates can be determined from stationary as well as from time-resolved fluorescence measurements. In the first case, the photon fluxes of donor (I_D) and acceptor (I_A) fluorescence are measured, and the ratio

$$I_A/I_D = \tau(\eta_A/\eta_D)\, k_{ET} \qquad (5)$$

can be calculated, assuming that the energy transfer rate k_{ET} is proportional to acceptor concentration,[22] and that the fluorescence quantum yields η_D and η_A of donor and acceptor molecules as well as the fluorescence lifetime τ of the donor are known. Another possibility of calculating k_{ET} is time-resolved fluorescence spectroscopy. If the fluorescence lifetime of a donor species is measured in the presence (lifetime τ) and in the absence (lifetime τ_0) of an acceptor, the energy transfer rate k_{ET} can be determined [considering eqn. (1)] by

$$1/\tau - 1/\tau_0 = k_{ET} \qquad (6)$$

Since k_{ET} depends on concentration of the acceptor species, increasing concentrations of DiI were used (see above).

Results

Fluorescence spectra of CHO cells cultivated for 24 h and incubated with laurdan for 60 min are depicted in Fig. 4. For whole cell illumination (Θ = 62°), the emission bands with maxima around 440 nm and 480–490 nm overlap, with the 440 nm band being more pronounced at 24 °C and the 480–490 nm band being predominant at 41 °C. In contrast, upon selective illumination of the plasma membrane (Θ = 66°) the short-wave emission band is predominant for all temperatures 24 °C ≤ T ≤ 41 °C (Fig. 4, lower curve). For quantitative evaluation, the generalized polarization[23] GP = (I_{440} − I_{490})/

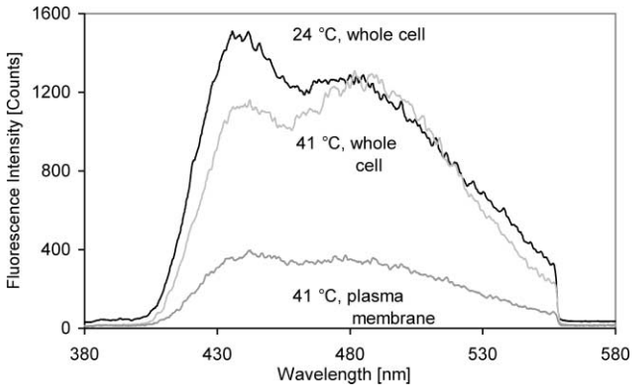

Fig. 4 Fluorescence spectra of CHO cells incubated with laurdan using either whole cell illumination (Θ=62°) at 24 or 41 °C or selective illumination of the plasma membrane (Θ=66°) at 41 °C.

(I_{440} + I_{490}) was calculated as an appropriate parameter of membrane dynamics with I_{440} corresponding to the fluorescence intensity at 440 nm and I_{490} to that at 490 nm. As depicted in Fig. 5, GP decreased with temperature between 24 and 41 °C from +0.09 to −0.01 for the plasma membrane and from +0.04 to −0.05 for the whole cell. GP generally increased during cell growth; all corresponding values after 48h of cell growth were about 0.02 units higher than those found after 24 h cultivation (data not shown).

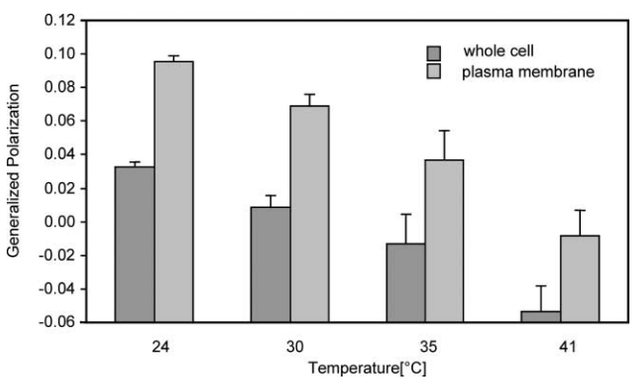

Fig. 5 Temperature dependence of generalized polarization GP=(I_{440} − I_{490})/(I_{440} + I_{490}) of laurdan fluorescence in single CHO cells grown for 24 h using either whole cell illumination (Θ=62°) or selective illumination of the plasma membrane (Θ=66°). Values represent median values and median absolute deviations (MADs) of 34–40 individual measurements in each case.

Fluorescence profiles of CHO cells incubated with laurdan (8 μM; 60 min) and excited by picosecond laser pulses (391 nm) are depicted in Fig. 6 for T = 24 and 35 °C using whole cell

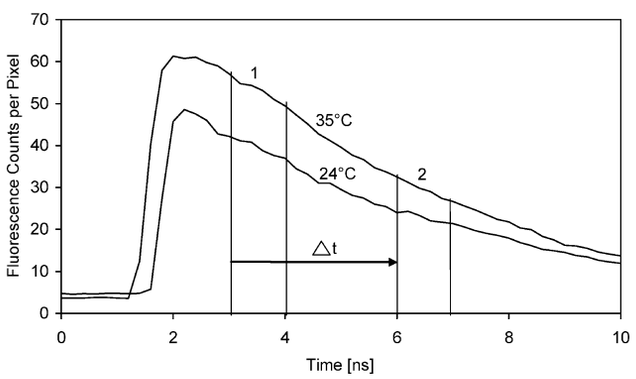

Fig. 6 Profiles of fluorescence increase and decay of CHO cells incubated with laurdan (8 μM; 60 min) at T=24 or 35 °C using whole cell illumination (Θ=62°) by picosecond laser pulses (λ_{ex}=391 nm; pulse duration: 55 ps). Profiles are obtained from an image of 220 × 160 μm in the spectral range of 420–800 nm. The time gates 1 and 2 and the time shift Δt used for fluorescence lifetime imaging are indicated.

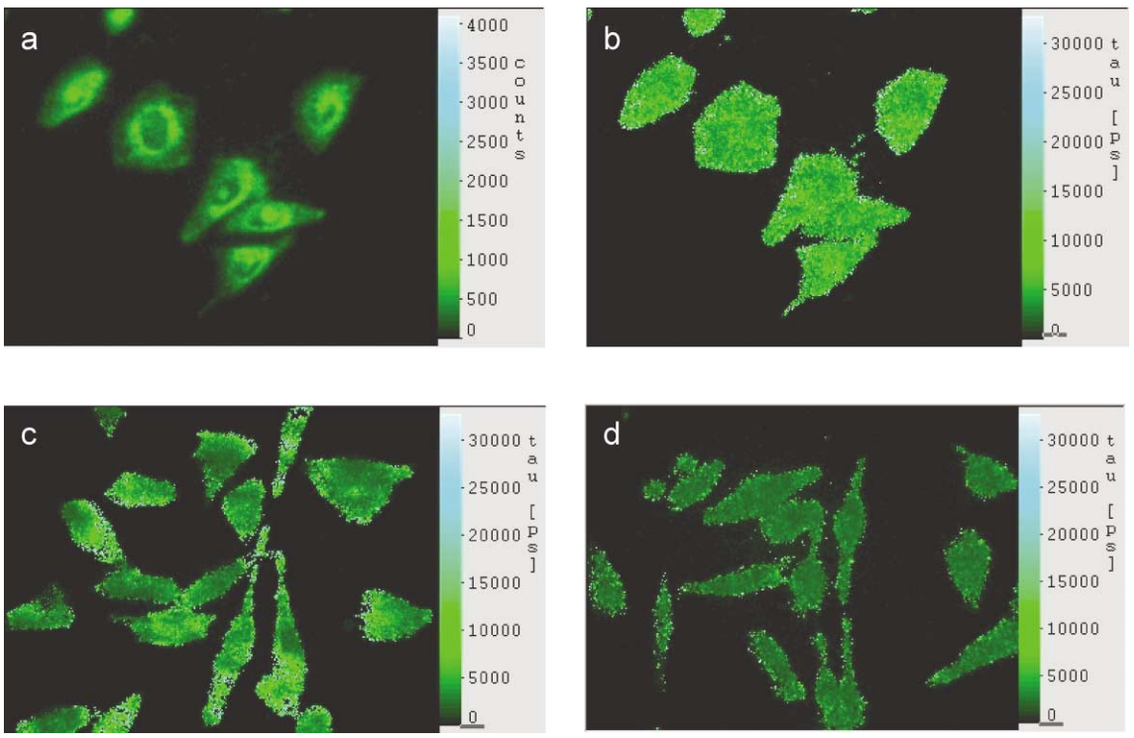

Fig. 7 Fluorescence intensity I_1 at 24 °C (a) and effective fluorescence lifetime τ_{eff} at 24 °C (b) or 35° C (c: young cells; d: aged cells) of CHO cells incubated with laurdan (8 μM; 60 min) using whole cell illumination ($\Theta = 62°$). Excitation wavelength: 391 nm; detection range: 420–800 nm; image size: 220 × 160 μm in each case).

illumination. From both curves fluorescence lifetimes around 5 ns can be deduced (24 °C: 5.8 ± 1.0 ns; 35 °C: 5.1 ± 0.6 ns). When fluorescence of the two emission bands was measured selectively in the spectral ranges of 454 ± 20 nm or 497 ± 20 nm, the lifetime of the short-wave band slightly decreased with temperature (by 20–30% between 24 and 41 °C), whereas the lifetime of the long-wave band remained almost constant. Fluorescence rise time at T = 24 °C occured within the experimental time resolution of 200 ps, whereas fluorescence onset at T = 35 °C was slightly delayed with a rise time of 0.5–0.8 ns. This result corresponds to earlier findings, where a single photon counting system with a time resolution around 100 ps (after deconvolution)[24] was used. Fluorescence intensity and lifetime images are depicted in Fig. 7. At both temperatures, the effective fluorescence lifetime τ_{eff} varied between about 2 and 8 ns for individual pixels (young cells; Fig. 7b,c). At T = 24 °C all effective lifetimes were uniformly distributed over the cells, whereas at temperatures above 30 °C domains with shorter and longer lifetimes could be distinguished. Domain patterns were not observed for aged cells (SC 35–38), where fluorescence lifetimes were again distributed uniformly over all cells (Fig. 7d). For all temperatures (24 °C ≤ T ≤ 41 °C) the fluorescence lifetime of aged cells was 3.3 ± 0.3 ns, *i.e.* considerably shorter than for younger subcultures.

Fluorescence spectra of single CHO cells incubated with either laurdan (8 μM) or DiI (8 μM) or coincubated with laurdan and DiI (8 μM each) are depicted in Fig. 8. In all cases the plasma membrane was illuminated selectively by an evanescent electromagnetic wave (Θ = 66°). Fig. 8 shows that laurdan fluorescence, but no DiI fluorescence is excited at 391 nm except from coincubation of laurdan and DiI. In this latter case the DiI emission band around 570 nm continuously increased, whereas laurdan fluorescence slightly decreased with acceptor concentration. This clearly proves that DiI fluorescence is excited *via* energy transfer from excited laurdan molecules with a rate k_{ET} increasing with DiI concentration. Concomitantly the fluorescence lifetime of laurdan (5.4 ns) decreased to 3.5 ns after conicubation with 8 μM DiI, such that according to eqn. (6) an energy transfer rate around 1.3×10^8 s^{-1} was determined.

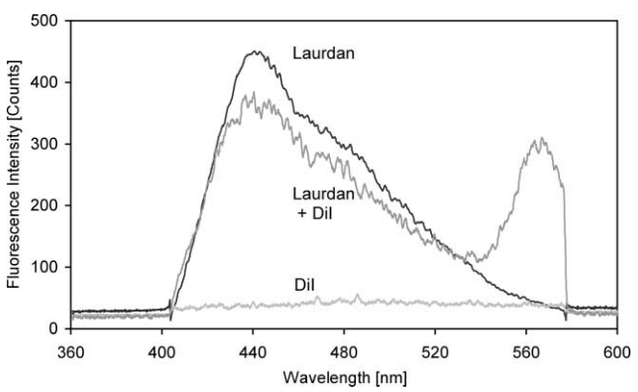

Fig. 8 Fluorescence spectra of CHO cells incubated for 10 min either with laurdan (8 μM) or with DiI (8 μM) or coincubated with laurdan and DiI (8 μM each) using selective illumination of the plasma membrane (Θ = 66°; λ_{ex} = 391 nm).

Discussion

A combination of microscopic techniques was used to characterize the fluorescent membrane marker laurdan. In the literature, the generalized polarization[23] as well as the fluorescence lifetime[15] have been reported to be appropriate parameters for membrane dynamics, *i.e.* membrane stiffness and fluidity. After incorporation into cell membranes, laurdan molecules show a fluorescence shift from about 440 to 490 nm when getting into contact with adjacent water molecules, *e.g.* when a phase transition from the tightly packed gel phase to the liquid crystalline phase of membrane lipids occurs. This effect is described by the generalized polarization (GP). In the present experiments, GP decreased with temperature, but increased with cell growth and was always higher after selective illumination of the plasma membrane than after illumination of the whole cell (including the plasma membrane and intracellular membranes), as also reported previously for BKEz-7 endothelial cells.[24] A higher stiffness of the plasma membrane as compared with intracellular membranes is probably due to a higher amount of cholesterol, as suggested in the literature[25]

and proven by preliminary measurements where the intracellular cholesterol content was modified (data not shown).

In addition to the generalized polarization, the fluorescence lifetime of laurdan appeared to be sensitive to the phase transition of membrane lipids, as first reported by Bagatolli *et al.*[15] This is proven by the fluorescence profiles at $T \geq 30$ °C, whose rise time of 0.5–0.8 ns may be related to a re-orientation of adjacent water dipoles during the lifetime of the excited state of the laurdan molecules. This dipole–dipole interaction usually occurs at higher temperature when membrane lipids are in the liquid-crystalline phase, but not within the tightly packed gel phase. The domain pattern of the effective fluorescence lifetimes shows that membrane properties vary within individual cells, and probably illustrates a different membrane composition. A shortening of the fluorescence lifetime and disappearance of the domain pattern for aged cells demonstrate that all membrane lipids are in the same phase at temperatures up to 41 °C. This is probably the gel phase, since the rise time of fluorescence profiles is infinetely short. A decrease of fluorescence lifetimes with temperature (as reported in the literature[15]) is less pronounced and only affects the short-wave band. This difference may be related to the more complex membrane structure of CHO cells in comparison with liposomes.[15]

The importance of TIRFM measurements should be emphasized, since membrane-associated fluorophores can be assessed more selectively than by any other microscopic technique, *e.g.* confocal or two-photon laser scanning microscopy.[26] Only in very few cases TIRFM has been combined with fluorescence lifetime[27,28] or FRET[29,30] measurements, so far. A combination of TIRFM and energy transfer experiments, however, appears particularly promising, since membrane markers can be examined in close proximity to an acceptor molecule. This has been tested for the acceptor DiI and may apply to various membrane proteins, *e.g.* ion channels or specific receptors after tracking with GFP or its mutants.

Only cell membranes in close proximity to a substrate (ventral membranes), but not dorsal membranes are assessed by TIRFM. This may be a disadvantage, if cells with asymmetric membranes or cell topologies are investigated. In addition to some confocal or near-field scanning techniques, dorsal membranes may be assessed by wide field microscopy using the method of structured illumination. If a structured object, *e.g.* diffraction grating is imaged in the plane of the sample, three images (shifted in phase) can be used to calculate an image from a well defined focal plane (*e.g.* dorsal cell membrane), whereas contributions of out-of-focus images vanish.[31] Corresponding images of CHO cells incubated with laurdan are reported elsewhere,[32] and further improvements of the structured illumination technique are described in the literature.[33]

Spectral properties, fluorescence lifetimes and energy transfer rates revealed to be main parameters for characterizing cell membranes, in particular membrane stiffness and fluidity. These membrane properties may have a large impact on the cellular uptake of various lipophilic molecules, *e.g.* pharmaceutical agents. In addition, membrane properties are expected to play a major role in pathogenesis of various diseases.

Acknowledgements

The authors thank the Bundesministerium für Bildung und Forschung (grant no. 1703201) and the Ministerium für Wissenschaft, Forschung und Kunst Baden-Württemberg (ZAF-Biotechnologie) for financial support, as well as Mrs C. Hintze for technical assistance.

References

1 J. R. Lakowicz, *Principles of Fluorescence Spectroscopy*, Plenum Press, New York–London, 1999.
2 H. Schneckenburger, R. Steiner, W. S. L. Strauss, K. Stock and R. Sailer, Fluorescence technologies in biomedical diagnostics, in *Handbook of Optical Biomedical Diagnostics*, ed. V. V. Tuchin, SPIE, Bellingham, WA, 2002, pp. 825–874.
3 T. Galeotti, G. D. V. van Rossum, D. H. Mayer and B. Chance, On the fluorescence of NAD(P)H in whole cell preparations of tumours and normal tissues, *Eur. J. Biochem.*, 1970, **17**, 485–496.
4 J.-M. Salmon, E. Kohen, P. Viallet, J. G. Hirschberg, A. W. Wouters, C. Kohen and B. Thorell, Microspectrofluorometric approach to the study of free/bound NAD(P)H ratio as metabolic indicator in various cell types, *Photochem. Photobiol.*, 1982, **36**, 585–593.
5 H. Schneckenburger, P. Gessler and I. Pavenstädt-Grupp, Measurements of mitochondrial deficiencies in living cells by microspectrofluorometry, *J. Histochem. Cytochem.*, 1992, **40**, 1573–1578.
6 I. Johnson, Fluorescent probes for living cells, *Histochem. J.*, 1988, **30**, 123–140.
7 J. M. Mullins, Overview of fluorochromes, *Methods Mol. Biol.*, 1999, **115**, 97–105.
8 R. Rizzuto, M. Brini, P. Pizzo, M. Murgia and T. Pozzan, Chimeric green fluorescent protein as a tool for visualizing subcellular organelles in living cells, *Curr. Biol.*, 1995, **5**, 635–642.
9 M. Ikawa, S. Yamada, T. Nakanishi and M. Okabe, Green fluorescent protein (GFP) as a vital marker in mammals, *Curr. Top. Dev. Biol.*, 1999, **44**, 1–20.
10 J. Pawley, *Handbook of Biological Confocal Microscopy*, Plenum Press, New York–London, 1990.
11 W. Denk, J. H. Strickler and W. W. Webb, Two-photon laser scanning microscope, *Science*, 1990, **248**, 73–76.
12 K. König, Multiphoton microscopy in life sciences, *J. Microsc.*, 2000, **200**, 83–86.
13 T. Parasassi, G. de Stasio, A. d'Ubaldo and E. Gratton, Phase fluctuation in phosopholipid membranes revealed by laurdan fluorescence, *Biophys. J.*, 1990, **57**, 1179–1181.
14 T. Parasassi, E. K. Krasnowska, L. Bagatolli and E. Gratton, Laurdan and prodan as polarity-sensitive fluorescent membrane probes, *J. Fluoresc.*, 1998, **4**, 365–373.
15 L. A. Bagatolli, T. Parasassi, G. D. Fidelio and E. Gratton, A model for the interaction of 6-lauroyl-2-(*N*,*N*-dimethylamino) naphthalene with lipid environments: implications for spectral properties, *Photochem. Photobiol.*, 1999, **70**, 557–564.
16 S. E. Sund, J. A. Swanson and D. Axelrod, Cell membrane orientation visualized by polarized total internal reflection fluorescence, *Biophys. J.*, 1999, **77**, 2266–2283.
17 K. Stock, R. Sailer, W. S. L. Strauss, M. Lyttek, R. Steiner and H. Schneckenburger, Variable-angle total internal reflection fluorescence microscopy (VA-TIRFM): realization and application of a compact illumination device, *J. Microsc.*, 2003, **211**, 19–29.
18 H. Schneckenburger, M. H. Gschwend, R. Sailer, H.-P. Mock and W. S. L. Strauss, Time-gated fluorescence microscopy in molecular and cellular biology, *Cell. Mol. Biol.*, 1998, **44**, 795–805.
19 D. Axelrod, Cell-substrate contacts illuminated by total internal reflection fluorescence, *J. Cell Biol.*, 1981, **89**, 141–145.
20 E. P. Buurman, R. Sanders, A. Draijer, H. C. Gerritsen, J. J. F. van Veen, P. M. Houpt and Y. K. Levine, Fluorescence lifetime imaging using a confocal laser scanning microscope, *Scanning*, 1992, **14**, 155–159.
21 T. Förster, Zwischenmolekularer Übergang von Elektronen-anregungsenergie, *Z. Elektrochem.*, 1960, **64**, 157–164.
22 H. Port, H. Schneckenburger and H. C. Wolf, Host–guest energy transfer *via* dipole–dipole interaction in doped fluorene crystals, *Z. Naturforsch.*, 1981, **36a**, 697–704.
23 T. Parasassi, G. de Stasio, G. Ravagnan, R. M. Rusch and E. Gratton, Quantitation of lipid phases in phospholipid vesicles by the generalized polarization of laurdan fluorescence, *Biophys. J.*, 1991, **60**, 179–189.
24 H. Schneckenburger, K. Stock, W. S. L. Strauss, J. Eickholz and R. Sailer, Time-gated total internal reflection fluorescence spectroscopy (TG-TIRFS): application to the membrane marker laurdan, *J. Microsc.*, 2003, **211**, 30–36.
25 T. Parasassi, M. diStefano, M. Loiero, G. Ravagnan and E. Gratton, Influence of cholesterol on phospholipid bilayers phase domains as detected by laurdan fluorescence, *Biophys. J.*, 1994, **66**, 120–132.
26 W. Yu, P. T. C. So, T. French and E. Gratton, Fluorescence generalized polarization of cell membranes: a two-photon scanning microscopy approach, *Biophys. J.*, 1996, **70**, 626–636.
27 S. Bicknese, N. Periasamy, S. B. Shohet and A. S. Verkman, Cytoplasmic viscosity near the cell plasma membrane: measurements by frequency domain microfluorimetry, *Biophys. J.*, 1993, **65**, 1272–1283.

28 H. Schneckenburger, K. Stock, M. Lyttek, W. S. L. Strauss and R. Sailer, Fluorescence lifetime imaging (FLIM) of rhodamine 123 in living cells, *Photochem. Photobiol. Sci.*, 2004, **3**, 127–131.
29 T. P. Burghardt and D. Axelrod, Total internal reflection study of energy transfer in surface-absorbed and dissolved bovine serum albumin, *Biochemistry*, 1983, **22**, 979–985.
30 A. S. Curtis, Cell reactions with biomaterials: the microscopies, *Eur. Cell Mater.*, 2001, **1**, 59–65.
31 M. A. A. Neil, R. Juskaitis and T. Wilson, Method of obtaining optical sectioning by structured light in a conventional microscope, *Opt. Lett.*, 1997, **22**, 1905–1907.
32 H. Schneckenburger, Optical Microscopy, in *Lasers and Current Optical Techniques in Biology*, ed. G. Palumbo and R. Pratesi, *Comprehensive Series in Photosciences*, Royal Society of Chemistry, Cambridge, 2004, **vol. 5**, pp. 331–355.
33 R. Heintzmann, T. M. Jovin and C. Cremer, Saturated patterned excitation microscopy – a concept for optical resolution improvement, *J. Opt. Soc. Am. A*, 2002, **19**, 1599–1609.